Ocean Dynamics (2002) 52: 116–122
DOI 10.1007/s10236-001-0009-9

Li Li · Thomas Pohlmann

The South China Sea warm-core ring 94S and its influence on the distribution of chemical tracers

Received: 16 May 2001 / Accepted: 5 November 2001

Abstract In this paper, the distributions of currents and chemical tracers were studied along two hydrographic sections across ring 94S, a warm-core ring found in the South China Sea. Results suggest that while currents on its offshore side maintained quasigeostrophic balance, such a balance was not reached on its onshore side. Therefore, it is suggested that interactions of ring 94S with the slope may play an important role: it may break down the quasigeostrophic balance and cause a deformation of the current field. The observed distribution of $\delta^{18}O$ supports the hypothesis that water masses inside the ring originate from the Kuroshio. Distributions of chemical tracers reveal a strong vertical disturbance of the isolines at the edge of ring 94S, where it approaches the shelf. This phenomenon may play an important role in the vertical exchange of biochemical elements across the thermocline. Possible reasons, i.e., enhanced vertical mixing and upwelling, are discussed.

Keywords South China Sea · Anticyclonic eddy · Nutrient distribution

1 Introduction

In September 1994, a warm-core ring was discovered near the continental slope of the northern South China Sea (SCS), and was discussed in detail for the first time (Li et al. 1997, 1998). Since rings may act as an important mechanism of the Kuroshio exchange with the SCS, this observation is crucial. This ring (ring 94S, named after the year and month of observation) is an anticyclone centered at about 21°N, 117.5°E, just off the continental slope with a horizontal scale of ~150 km and a vertical scale of 1000 m. Near-surface current speeds of about 1 m s^{-1} were estimated from both ADCP measurements and geostrophic calculations. Analysis of chemical parameters suggested that ring 94S originates from the Kuroshio, which is in line with findings of McWilliams and Flierl (1979) that anticyclonic eddies move predominantly westward. Numerical experiments of Smith (1986) indicate that this phenomenon of eddy intrusion is not confined to the SCS. Smith (1986) applied his model to the Gulf of Mexico, where eddies originating from the warm loop current intrude into the western Gulf of Mexico. This situation seems to be very similar to that in the northeastern SCS, where rings detached from the Kuroshio are also supposed to propagate towards the northwest.

The September 1994 survey was conducted with four research vessels (see Li et al. 1998, for details). Figure 1 shows the distribution of CTD stations together with the surface geopotential anomalies in dynamic meters referred to 500 db. The geopotential anomaly field in shallower regions was integrated by additionally using the dynamic height information from the nearest deep water station. The procedure is described in more detail in Li et al. (1998). The 100-m isobath is shown in Fig. 1 as a broken line to outline the extension of the shelf. Due to the fact that September marks the transition season between the two monsoon phases, the general situation in this month is characterized by a weak and unstable circulation pattern in the investigation area. The dynamic heights presented in Fig. 1 indicate that at the time of observation this typical unstable background flow was also present. Additionally, an anticyclonic ring appeared, which was situated very close to the steep slope and elongated along the isobaths. As stated by Cushman-Roisin (1986), the stability of anticyclonic eddies of realistic size decreases with increasing

Responsible Editor: Jean-Marie Beckers

L. Li
The Third Institute of Oceanography,
State Oceanic Administration,
P.O.Box 0570, Xiamen, 361005, China
e-mail: lili@xmu.edu.cn

T. Pohlmann (✉)
Institute of Oceanography,
University of Hamburg,
Troplowitzstr. 7, 22529 Hamburg, Germany
e-mail: pohlmann@ifm.uni-hamburg.de

eccentricity. Another potential source of instability is the strong interaction with topography, which can be expected when the ring wall hits the bottom.

Previous publications related to ring 94S (Li et al. 1997, 1998) have placed their main focus on proving the existence of the ring itself, whereas the current paper tries to investigate the related processes by using ADCP current measurements and chemical tracer distributions along sections A and B, both crossing ring 94S (Fig. 1). While section A crossed the ring along its main axis basically, section B was oriented offshore and cut the ring through its southwestern corner only.

2 Current fields

Geostrophic currents relative to 500 db were estimated from CTD measurements along sections A and B against pressure (Fig. 2a, b). For stations where the bottom depth is shallower than 500 db, current speeds were estimated from the geopotential anomaly fields integrated along the bottom. For stations where the CTD cast did not reach 500 db, values below the maximal depth of the cast were adopted from the nearest deeper station along the section.

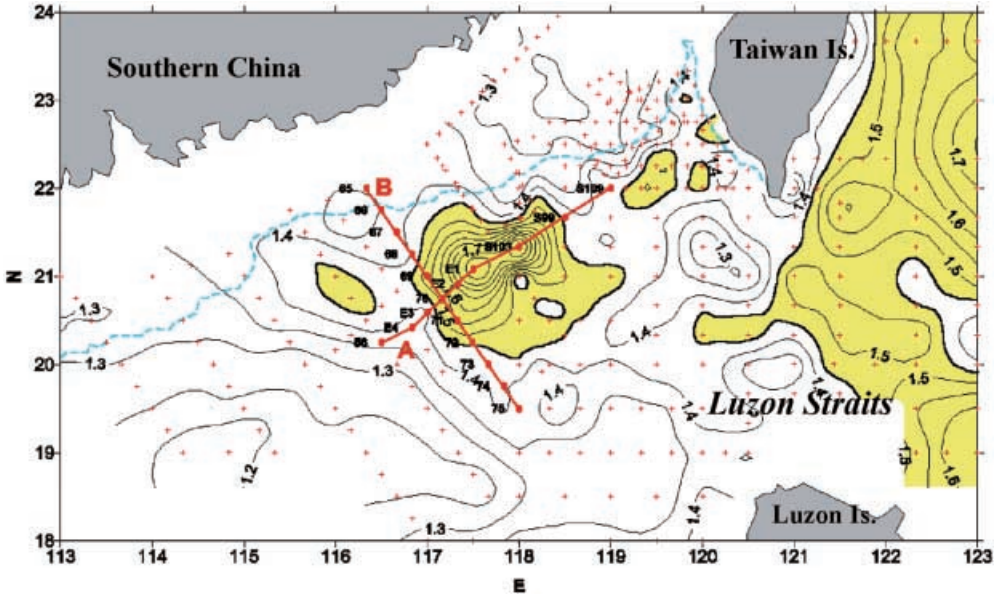

Fig. 1 Surface geopotential anomaly referred to 500 db (in dynamic meters) with CTD stations posted; the *broken line* shows the position of shelf break

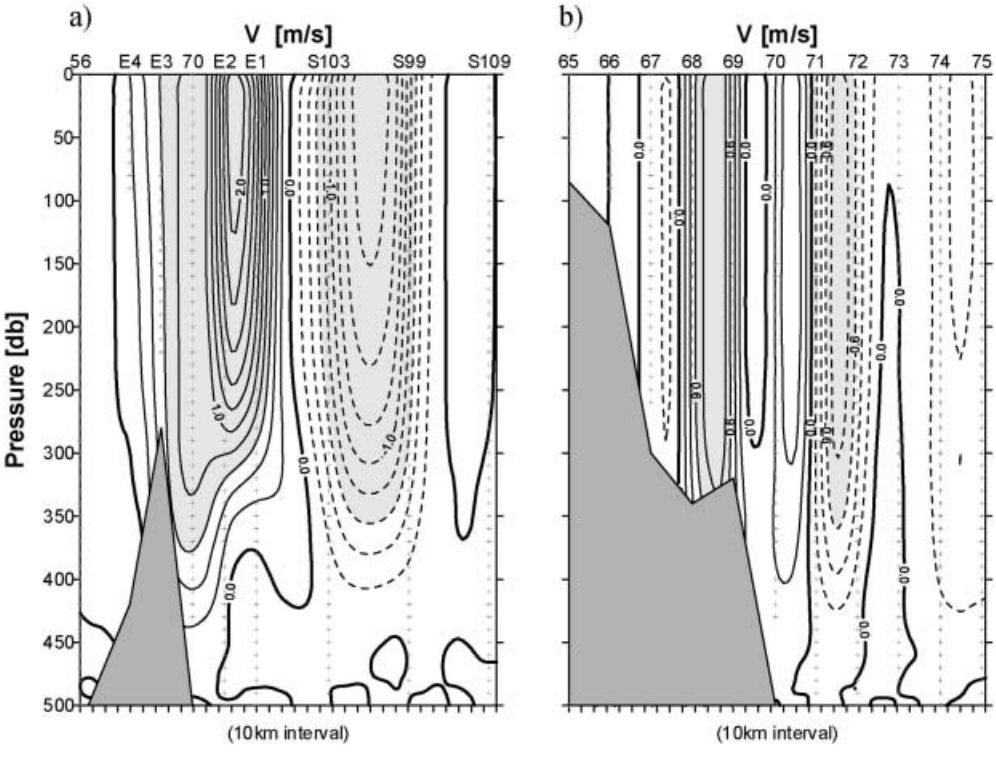

Fig. 2a, b Distribution of geostrophic currents along **a** section A and **b** section B

Both figures show a typical eddy structure with geostrophic currents reversed across the section in an anticyclonic manner. Maximal geostrophic currents of swirling were observed from stations E2 to E1 (>2.0 m s^{-1}) and from S103 to S99 (>1.8 m s^{-1}) in section A, and from stations 68 to 69 (>0.8 m s^{-1}) and from stations 71 to 72 (>0.8 m s^{-1}) in section B. Currents appeared to be stronger near the surface. Since section A crossed the ring near its main axis and section B cut the ring only through its southwestern end, it is not surprising that geostrophic currents observed along section A are much stronger than those of section B. The long-shore scale of the ring estimated from Fig. 2a is about 180 km.

In comparison, ADCP measurements showing the flow perpendicular to section A and B are presented for the upper 240 m of the water column (Fig. 3). Unfortunately, ADCP measurements are not available for the full sections but only from stations E4 to E1 and stations 71 to 75 for section A and B, respectively.

It can be observed that the ADCP measurements from stations E4 to E1 of section A (Fig. 3a) are quite different from geostrophic estimates (Fig. 2a). The ADCP measurements show a much weaker current. The observed maximal current perpendicular to the section derived from the ADCP measurements is about 0.3 m s^{-1} compared to 2 m s^{-1} from the geostrophic computation. Presently, it is not fully clear what is causing this discrepancy. However, it is obvious that the onshore sector of ring 94S (northeast to section A) was sitting over the slope (Fig. 2b), and the southwestern ring wall was in contact with a shallow ridge (Fig. 2a). Hence, interactions of ring 94S with the topography may play an important role in the sense that the quasigeostrophic balance breaks down and causes a deformation of the current field. Recent results from LaCasce (1998) also indicate that deep-reaching eddies are significantly dispersed on hitting the continental slope.

In contrast, ADCP measurements along section B between stations 71 and 75 (Fig. 3b) agree quite well with geostrophic estimation (Fig. 2b), suggesting a quasigeostrophic nature on the offshore side of the ring where the water is deep enough and the ring does not interact strongly with the bottom.

Several mechanisms may cause a decay of mesoscale eddies when they interact with topographic features (Smith 1983). When rings approach the continental margin, the movement of the vortex column across the isobaths will generate topographic Rossby waves or coastal trapped waves, as stated by Grimshaw et al. (1994). The dispersion properties of both types of these waves are governed primarily by the topography. The energy available from rings may propagate away from the rings and may be refracted, reflected, and/or scattered over the steep slope. All analytical solution which have been proposed in this context, i.e., Grimshaw et al. (1994) or LaCasce (1998), apply only to the inviscid equations of motion for their studies. Therefore, from theory, no information about the influence of bottom friction can be obtained. However, it can be assumed that for deep-reaching eddies hitting the topography, bottom friction can also cause a direct damping of the flow.

Another process that could explain the loss of energy of the ring is internal wave activity generated at the ring walls, when the ring hits the slope. Observations support this hypothesis, since they frequently show episodic diurnal oscillation of the baroclinic current over the shelf about 100 nautical miles west of the ring (G. Fang, personal communication). Moreover, strong internal solitons are frequently observed in this area (Liu et al. 1998).

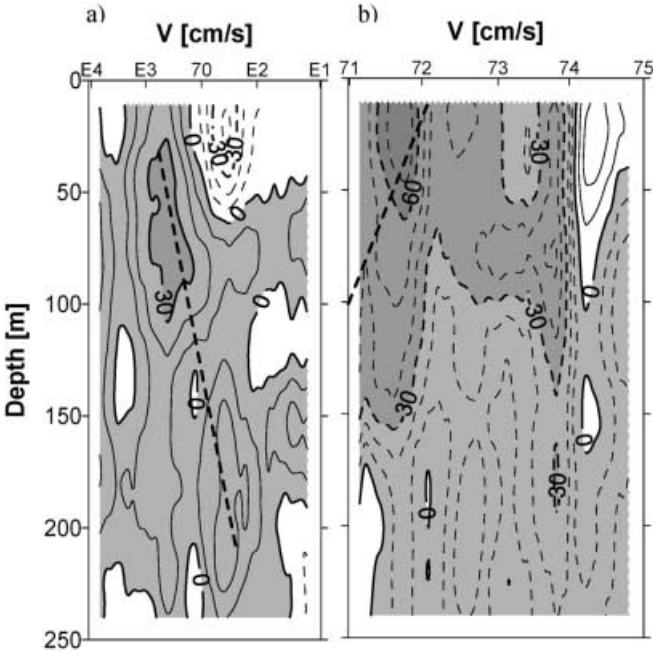

Fig. 3a, b Distribution of ADCP currents perpendicular to the section measured **a** from stations E4 to E1 along section A and **b** from stations 71 to 75 along section B; *positive values* indicate northward flow

3 Results of tracer measurements

During the 1994 survey, water samples were taken at selected stations for the analysis of chemical tracers including nutrients, dissolved oxygen, and ^{18}O (a stable isotope of oxygen). Contents of nutrients and dissolved oxygen were measured using standard analytical techniques (Han 1986). Concentration of ^{18}O was measured by its richness relative to ^{16}O defined as $\delta^{18}O = [(^{18}O/^{16}O)_{sample}/(^{18}O/^{16}O)_{smow} - 1] \times 10^3$, where SMOW is the abbreviation for Standard Mean Ocean Water. Please refer to Hong et al. 1997 for details of the method and general results of the $\delta^{18}O$ measurement.

Contours of concentration of these tracers across the southwestern ring wall (from stations E4 to E2 along section A, see Fig. 1) are presented in Fig. 4 together with contours of temperature and salinity for comparison. The interpolation between data points, indicated by

crosses, is performed by means of the kriging method. This method has the property that the values at data points are reproduced exactly, which sometimes causes too strong local extrema. However, the general patterns are correct and since all parameters of Fig. 4 are treated with the same method, the interpretation is not greatly affected by the choice of interpolation scheme.

The ring is characterized by a sharp vertical displacement of the thermocline between stations E2 and E1 (Fig. 4a), where the most energetic currents were observed (see Fig. 2a). Some contours are shaded in these figures to highlight features of property distributions. The general distribution of salinity, dissolved oxygen, and $\delta^{18}O$ below 100 m is somewhat similar to that of temperature. Both salinity and $\delta^{18}O$ show a layer of maximum concentration along the thermocline (Fig. 4b and d, shaded). Salinity within this layer is higher than 34.7 psu, which corresponds to values found inside the ring core and is probably originating from the Kuroshio (>34.7 psu at 150 m, according to Shaw 1989). $\delta^{18}O$ values higher than 0.3 also form a layer of maximum concentration aligned with the thermocline, though its contours dome up around station 70.

Distributions of all three nutrients show evident features around station 70. A doming of isolines of $[PO_4]$ and $[SiO_4]$ was observed with a vertical band of low $[NO_2]$ at the central part of the section. Similar features can also be found in the contours of dissolved oxygen and $\delta^{18}O$, but they are less distinctive. The mixing diagrams of P over S (Fig. 5a) and of Si over S (Fig. 5b)

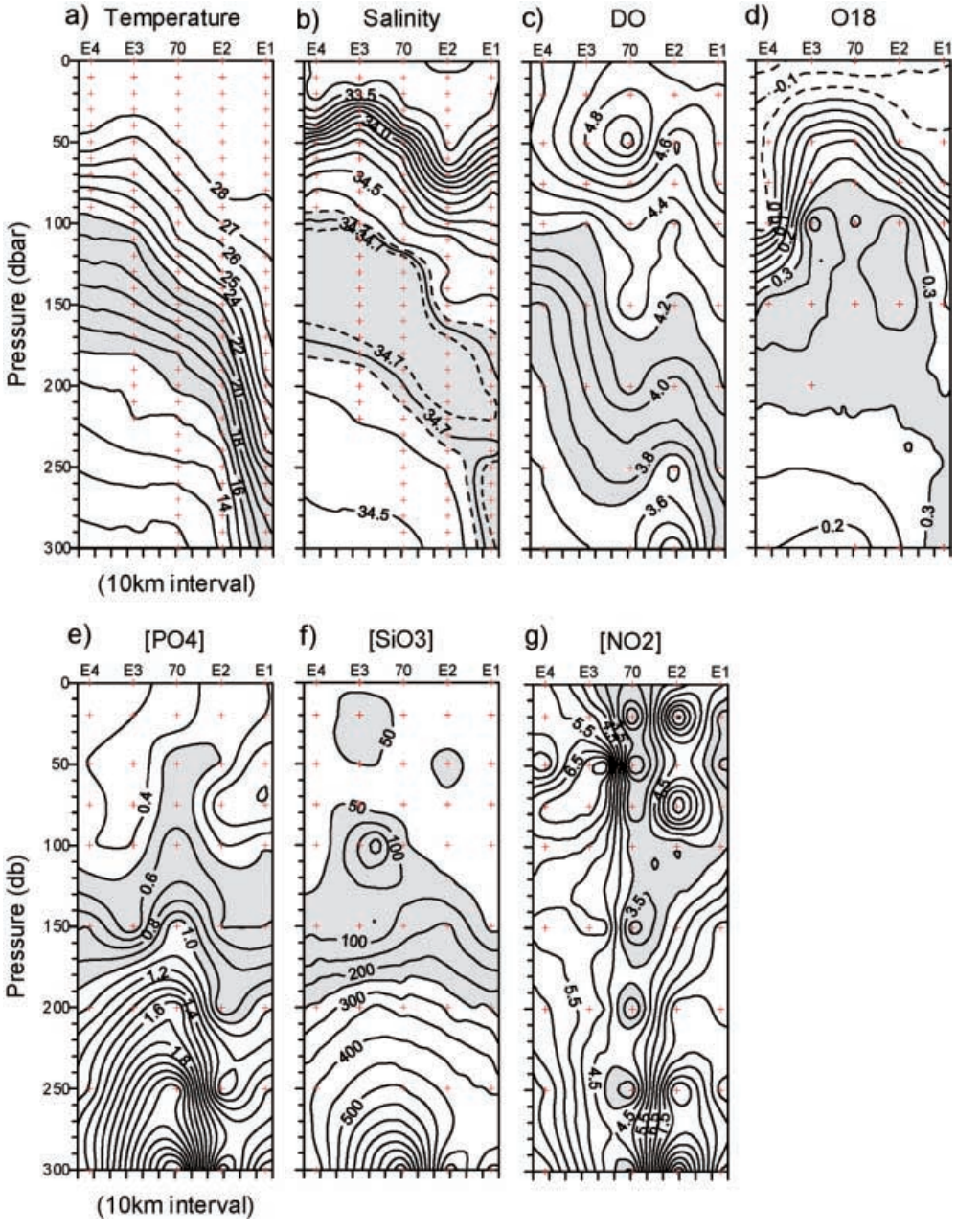

Fig. 4a–g Distributions of temperature, salinity, and concentration of chemical tracers along section A from stations E4 to E1 showing "stirring effect" at the outer edge of ring 94a. **a** Temperature (°C). **b** Salinity (psu). **c** Dissolved oxygen (ml l^{-1}). **d** $\delta^{18}O$. **e** Phosphate (μg l^{-1}). **f** Silicate (μg l^{-1}). **g** Nitrite (μg l^{-1})

indicate that three types of water masses, i.e., (1) low nutrients – low salinity, (2) high nutrients – high salinity, and (3) low nutrients – highest salinity, are present. These three types have their origin in (1) the SCS surface waters, (2) the SCS intermediate waters, and (3) very likely from the Kuroshio. Both mixing diagrams indicate that no direct mixing between the intermediate water and the surface water occurs. On the other hand, the mixing diagram DO over S shows an inverse distribution (Fig. 5c). Both Kuroshio and surface water have high DO concentrations, whereas low DO concentrations are found for the intermediate water. This inverse behavior compared to the nutrients is in line with the assumption that in the euphotic zone high nutrient concentrations are correlated with low oxygen concentrations and vice versa. Below the euphotic zone, i.e., in the SCS intermediate water, nutrient concentrations are high, since nutrients leaving the surface layer are concentrated here because, due to the light limitation, no biological uptake occurs. On the other hand, DO concentrations are smaller because the intermediate water has no direct contact with the sea surface. For nitrite, the situation is totally different (Fig. 5d). No distinct correlation between N and S can be found. Interestingly, at station 70 nitrite exhibits small concentrations for all waterbodies (cf. Fig. 4g).

4 ^{18}O and its indication of Kuroshio water

^{18}O has been used as a tracer of water mass since the late 1970s (Tan and Strain 1980; Huang et al. 1996). The content of ^{18}O in the ocean is governed by fractionation during evaporation and sea-ice formation and by inputs of isotopic content from precipitation and runoff. As a heavier isotope, ^{18}O is enriched in seawater due to evaporation because ^{16}O is preferentially evaporated, since the light molecules of $H_2{}^{16}O$ tend to evaporate first. As freshwater originates from evaporated seawater, the concentration of ^{18}O in freshwater is relatively low. Influenced by river runoff, values of $\delta^{18}O$ are usually negative in continental shelf areas. In contrast, in subtropical open oceans, surface values are mostly

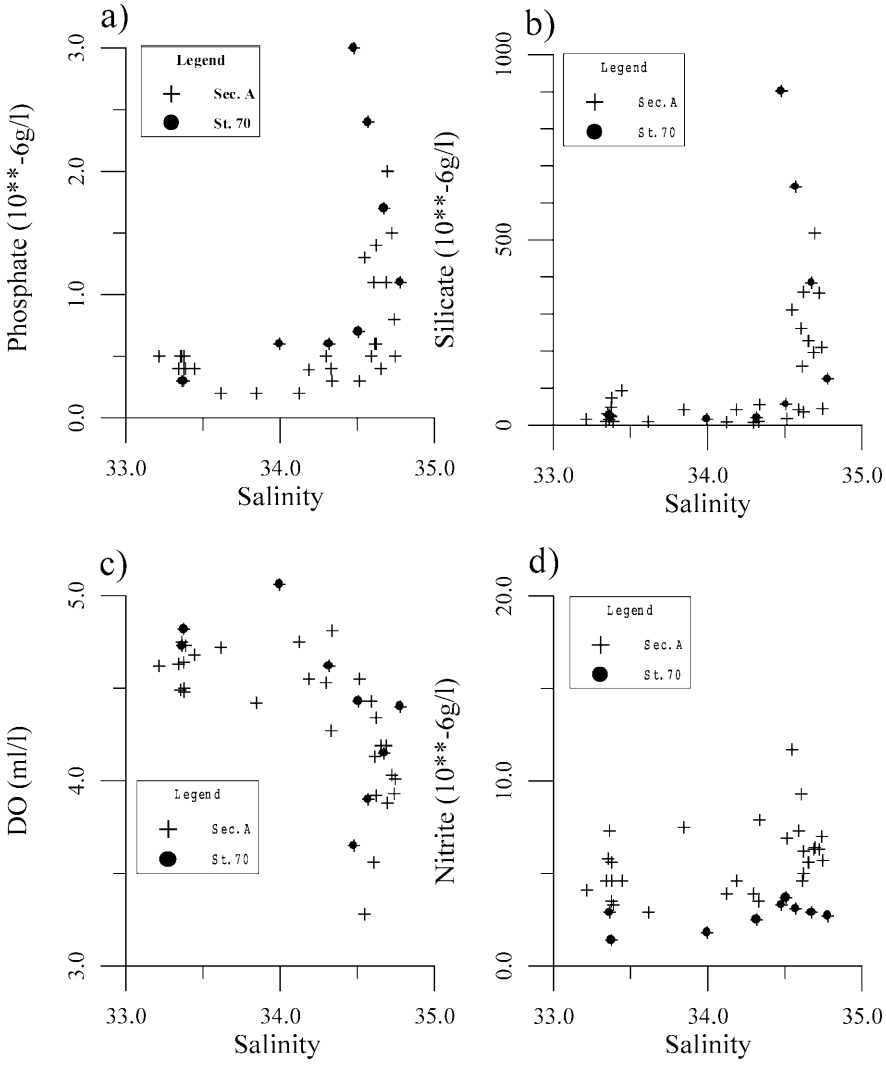

Fig. 5a–d Mixing diagrams along section A against salinity (psu). **a** Phosphate (μg l^{-1}). **b** Silicate (μg l^{-1}). **c** Dissolved oxygen (ml l^{-1}). **d** Nitrite (μg l^{-1}). Station 70 highlighted by *circles*

positive, reflecting the dominance of evaporation (Schmidt 1998).

Over the northern continental shelves of the South China Sea, $\delta^{18}O$ is reported to be low (Li and Hong 1991; Huang et al. 1996; Hong et al. 1997). High $\delta^{18}O$ values, however, are observed in the equatorial western Pacific near the Philippines, showing a maximum at the subsurface (Hong et al. 1999). The $\delta^{18}O$ maximum layer is associated with the core layer of saline North Pacific Central Water (NPCW), which is formed in the central North Pacific by strong evaporation. Subsequently, NPCW spreads out and moves with the northern subtropical gyre (Pickard and Emery 1982) to the western boundary of the North Pacific, where a small amount finally enters the South China Sea through the Luzon Straits (Wyrtki 1961). Hence, ^{18}O can be is used as a tracer of Kuroshio water in the South China Sea. Huang et al. (1996) conducted intensive $\delta^{18}O$ measurements in waters of the northeastern South China Sea in March 1992. They showed a $\delta^{18}O$ maximal layer lying at $\sim$100 m depth with values increasing eastward from 0.30 at 113°E to 0.64 in the northern Luzon Straits, and suggested that $\delta^{18}O > 0.4$ may be used to identify of Kuroshio subsurface water in the South China Sea.

In our previous analysis of hydrographic datasets from the same survey (Li et al. 1997; 1998), we showed that water masses inside the ring are different from those of the South China Sea and so we suggest that they originate from the Kuroshio. The respective end member of the *T–S* diagram (Fig. 6) has a salinity of 34.9 psu and a temperature of 26°C, which coincides nicely with characteristics of Kuroshio water in the assumed separation area. This viewpoint is further supported here by distributions of $\delta^{18}O$ (Fig. 4d), which show values inside the ring wall (above the thermocline) higher than 0.4 and inside the ring core with values above 0.3. A higher values would be expected further east along the section; unfortunately, no subsurface measurements were carried out east of station E1 during the survey.

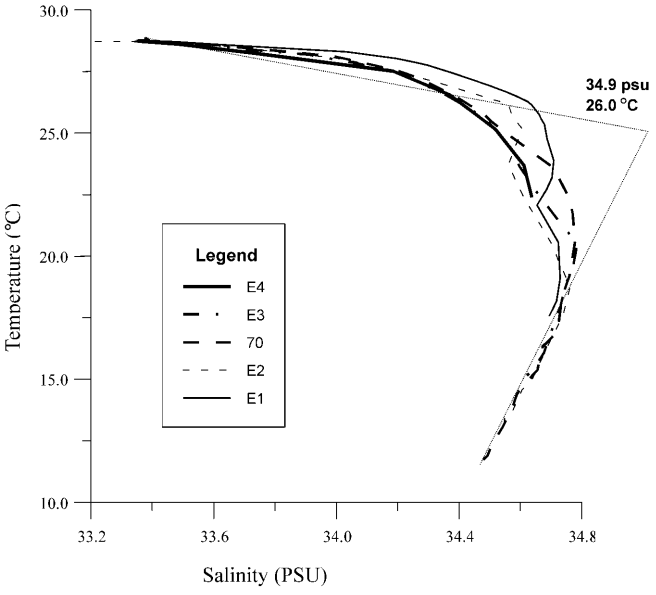

Fig. 6 *T–S* diagrams for stations E1, E2, 70, E3, and E4

5 The "stirring" effect

A very striking feature of the nutrient distributions is their symmetry around station 70 (Fig. 4), which is located at the edge of the ring (Fig. 1) just outside its strong shear zone (Fig. 2a). Contours of phosphate and silicate protrude upward near station 70 (Fig. 4e), while those for nitrite show minimum concentrations over the entire water column. Similar features can also be seen in Fig. 4c and d where oxygen maxima appear at station 70, and minimum $\delta^{18}O$ concentrations appear at the center of the dome mentioned in section 3.

One can speculate which is the dominant process that causes this symmetric feature of the tracer distributions. Although up to now no final conclusion has been drawn, it is quite clear, however, that this phenomenon is associated with the ring wall. Since for temperature and salinity a comparable uplift can be found for all sections crossing the eddy also from other directions (Li et al. 1998), it can be excluded that the structures displayed in Fig. 4 are snapshots of internal waves. Most likely, enhanced vertical mixing at the outer edge of the ring is responsible for the uplift of the Kuroshio water characteristics into the upper surface layer. Moreover, this strong vertical mixing could also be one reason for the discrepancy between the geostrophic current velocities and the flow measured with the ADCP, since for this deep-reaching eddy, vertical friction seems to be an effective way to lose kinetic energy. In other words, this additional frictional force can be responsible for the disturbance of the geostrophic balance.

This enhanced vertical mixing process causes an upward entrainment of nutrient-rich water and a downward transport of oxygen-rich water along the ring wall. Vertical mixing may also reduce the content of $\delta^{18}O$ in the center of the dome (Fig. 4d), since water in upper layers is more $\delta^{18}O$-depleted. On the other hand, increasing gradients of P and Si between 200 and 300 m around station 70 indicate that, below the thermocline, upwelling becomes increasingly important with depth. At present it is not clear whether this upwelling is caused because the ring hits the sloping bottom or whether it is a general phenomenon connected with instabilities at the ring wall which were simulated, for example, by McGillicudy et al. (1995). Here, additional numerical studies are needed to elucidate the situation.

For nitrite, these purely physical arguments cannot explain the observed distribution. Here, additional chemical and biological processes have to be considered. The balance between different nitrogen forms strongly depends on the hydrographic conditions and the biological productivity. Nitrite can be derived from either the oxidation of ammonia or the reduction of nitrate, and can be removed during nitrogen assimilation by

phytoplankton or by oxidation (Vaccaro 1965). Specifically, both the increase of dissolved oxygen by vertical mixing and the uplift of the thermocline (and thus the pycnocline where phytoplankton stays) observed around station 70 are in favor of nitrite oxidation. Hence, a column of minimum nitrite concentrations may occur. More insight into this hydrodynamical–chemical–biological system could be provided by an application of a coupled model, like that of McGillicudy et al. (1995). Interestingly, these authors made the first tests of their coupled physical–biological model for an isolated vortex. However, since they used typical North Atlantic conditions in their simulation, their results cannot be transferred directly to the situation found at ring 94S.

Thus, it is suggested that strong mixing at the ring wall plays an important role in the vertical exchange of biochemical elements across the thermocline. In other words, there exists a strong ''stirring effect'' where rings and their surrounding waters interact. This finding is supported by numerical results obtained by Kroll (1993), who came to the conclusion that under realistic conditions, instabilities of warm-core eddies are confined to the outer edge of the eddy, i.e., the ring wall. In the specific case of ring 94S the transport of nutrients into this ''stirring zone'' seems to be caused by upwelling occurring below the thermocline.

6 Summary

1. Analyses reveal that ring 94S is subject to strong dispersion approaching the continental slope. While currents on its offshore side maintain quasigeostrophic balance, this balance is not observed near the slope.
2. Results of ^{18}O measurement support the viewpoint from T–S analyses that water masses inside the ring originate from the Kuroshio.
3. Distributions of chemical tracers at the outer edge of the ring wall reveal enhanced vertical mixing in the upper layer in combination with upwelling below the thermocline.
4. Additional numerical studies are necessary to understand the processes responsible for the dispersion of rings and the upward movement of tracers, and to quantify the contributions of bottom friction and upwelling to these phenomena.

Acknowledgements This work was supported by the Chinese National Science Foundation project no. 49976010 and by the Chinese National Key Programme for Developing Basic Sciences project no. G1999043807. The paper was prepared in the framework of the German-Chinese Cooperation in Marine Science and Technology under the project no. CHN 98/017. The observation used in this study was carried out in the framework of the Chinese National Science Foundation project no. 49456001. Scientists and crew members who participated in the field study are gratefully acknowledged. Special thanks go to Dr. Joe Wang of NTU for kindly providing his CTD data, to Professor Hong A'shi of TIO/SOA and Professor Wu Linxing of SCSIO/CAS for conducting tracer measurements, and to Dr. Dai Minhan of XMU for his valuable comments on this manuscript. Finally, we should like to thank our colleagues Jing Chunsheng and Wu Risheng for their very helpful support.

References

Cushman-Roisin B (1986) Linear stability of large, elliptical warm-core rings. J Phys Oceanogr 16: 1158–1164

Grimshaw R, Broutman D, He X, Sun P (1994) Analytical and numerical study of a barotropic eddy on a topographic slope. J Phys Oceanogr 24: 1587–1607

Han (1986) Manual of survey for water chemistry elements (in Chinese). Ocean Press, Bejing, 263 pp

Hong A, Huang Y, Hong Y et al (1999) Distributive characteristics of oxygen isotope of sea water from north of Solomon Is. and west of Guam (in Chinese with English abstract). Oceanogr China 10: 60–65

Hong A, Hong Y, Ke J et al (1997) Distributive characteristics of O isotope of the northeastern South China Sea in the summer of 1994 (in Chinese with English abstract). Trop Oceanol 16(2): 82–89

Huang Y, Shi W, Jin D et al (1996) The distributions of ^{18}O in the waters of the northeastern South China Sea (in Chinese with English abstract). Oceanogr China 6: 82–92

Kroll J (1993) The stability of an axially symmetric warm-core model eddy on a stratified ocean. J Mar Res 51: 273–292

LaCasce JH (1998) A geostrophic vortex over a slope. J Phys Oceanogr 28: 2362–2381

Li W, Hong H (1991) The characteristics of ^{18}O distribution in the southern Taiwan Strait and its tracer study in water masses (in Chinese with English abstract). In: Hong H, Ruan W, Hong G (eds) Minnan-Taiwan Bank fishing ground upwelling ecosystem study. Science Press, Beijing 307–313

Li L, Su J, Xu J (1997) Detached Kuroshio rings in the South China Sea (in Chinese with English abstract). Trop Oceanol 16(2): 42–57

Li L, Nowlin WD Jr, Su J (1998) Anticyclonic rings from the Kuroshio in the South China Sea. Deep-Sea Res (Part I) 45: 1469–1482

Liu AK, Chang YS, Hsu M-K et al (1998) Evolution of nonlinear internal waves in the East and South China Seas. J Geophys Res 103(C4): 7995–8008

McWilliams JC, Flierl GR (1979) On the evolution of isolated, nonlinear vortices. J Phys Oceanogr 9: 1155–1182

McGillicuddy DJ, Robinson AR, McCarthy JJ (1995) Coupled physical and biological modelling of the spring bloom in the North Atlantic (II): three-dimensional bloom and post-bloom processes. Deep-Sea Res (Part I) 42: 1359–1398

Pickard GL, Emery WJ (1982) Descriptive physical oceanography, an introduction, 4th enlarged edn. Pergamon Press, Oxford, 249 pp

Schmidt GA (1998) Oxygen-18 variation in a global ocean model. Geophys Res Lett 25: 1201–1204

Shaw P-T (1989) The intrusion of water masses into the sea south west of Taiwan. J Geophys Res 94(C12): 18213–18226

Smith DC (1986) A numerical study of loop current eddy interaction with topography in the western Gulf of Mexico. J Phys Oceanogr 16: 1260–1271

Smith PC (1983) Eddies and coastal interactions. In: Robinson AR (ed) Eddies in marine science. Springer Berlin Heidelberg New York, pp 446–480

Tan FC, Strain PM (1980) The distributions of sea ice meltwater in the Eastern Canadian Arctic. J Geophys Res 85(C4): 1925–1932

Vaccaro RF (1965) Inorganic nitrogen in sea water. In: Riley JP, Skirrow G (eds) Chemical oceanography, vol. 1 Academic Press, London 365–408

Wyrtki K (1961) Scientific results of marine investigations of the South China Sea and the Gulf of Thailand 1959–1961. Naga Rep vol 2